The International Journal of Advanced Manufacturing Technology (2019) 104:301–313
https://doi.org/10.1007/s00170-019-03668-4

ORIGINAL ARTICLE

Research on homogenization and surface morphology of Ti-6Al-4V alloy by longitudinal-torsional coupled ultrasonic vibration ball-end milling

Wanfei Ren[1,2] · Jinkai Xu[1] · Jieqiong Lin[2] · Zhanjiang Yu[1] · Peng Yu[1] · Zhongxu Lian[1] · Huadong Yu[1]

Received: 13 December 2018 / Accepted: 27 March 2019 / Published online: 31 May 2019

Abstract
This research studied the surface homogenization and morphology of a Ti-6Al-4V alloy using the longitudinal-torsional coupled ultrasonic vibration-assisted milling (UVAM) of a ball-end cutter, in which a method of continuous processing between the flat surface and the freeform surface connection was proposed. The cutting experiments compared the UVAM method with the conventional milling (CM) process by setting three parameters: the cutting speed, feeding rate, and depth of cut. The finished surface roughness, the in situ cutting force, and the topography of the surface are characterized in this paper. The surface roughness that resulted from UVAM ball-end milling was much better than the surface roughness of CM at high cutting speeds. In particular, there was a steep decrease of the average roughness rate from 0.668 μm at 4000 rpm to 0.161 μm at 5000 rpm. Moreover, the mean cutting force in ball-end milling using UVAM decreased by 20–40% compared to the CM process. The homogenization of the surface roughness also improved from 59.4 to 15.1% in the UVAM method compared to the CM method when the transverse-longitudinal ratio was taken into consideration. The cutting experiments have not only powerfully demonstrated the validity of the UVAM method but have also shown the beneficial effect that the UVAM process brings.

Keywords Ultrasonic vibration-assisted milling (UVAM) · Homogenization · Ball-end milling · Surface morphology · In situ cutting force

1 Introduction

Recently, because it is one of the tough materials [1, 2], Ti-6Al-4V (α-β titanium alloy) has been widely applied in aeronautics and astronautics, defense, medical apparatuses, energy, and other fields due to its high-strength superior mechanical and chemical properties (high hardness, high rigidity, excellent wear, and corrosion resistance). However, Ti-6Al-4V generates a large amount of cutting heat in the conventional cutting processes [3, 4]. For instance, the tool wear [5] was severe for conventional milling. UVAM (a kind of longitudinal-torsional ultrasonic vibration-assisted milling in which the torsional vibration is a by-product of the longitudinal vibration caused by the spiral groove on the milling cutter) became an effective method when ultrasonic vibration assistance [6] was applied for CM. Numerous research studies have focused on ultrasonic vibration-assisted turning [7, 8], drilling [9, 10], and grinding [11, 12], but few studies have focused on UVAM. UVAM not only has the advantages of a high-frequency response and a reduction of the cutting force, but it also plays a significant role in reducing the roughness of the machining surface, reducing the temperature in the cutting region, improving the processing efficiency and extending the service life of the tool.

Ball-end milling [13] is necessary for conducting fine milling for the last step of complex surfaces, including flat

Electronic supplementary material The online version of this article (https://doi.org/10.1007/s00170-019-03668-4) contains supplementary material, which is available to authorized users.

✉ Jinkai Xu
xujinkai2000@163.com

[1] National and Local Joint Engineering Laboratory for Precision Manufacturing and Detection Technology, Changchun University of Science and Technology, Changchun 130012, China

[2] School of Mechatronic Engineering, Changchun University of Technology, Changchun 130012, China

surfaces and freeform surfaces. In an ordinary three-axis milling machine, ball-end milling can process only incline and freeform surfaces rather than flat surfaces. The reason for this is that the cutting speed is almost zero in the center of the ball-end milling cutter, which has an adverse effect on the surface quality. Surface roughness has improved significantly with the use of UVAM in planar precision milling, with no tilting the of ball-end mill needed. Recently, there has been much study of ball-end milling, including the establishment of the ball-end milling process with a straight tool paths model [14], developing a new numerical model to define the surface morphology [15], and inventing a feasible method to predict the surface roughness [16]. However, for the ball-end milling of the CM applications in the above references, UVAM was rarely seen. Additionally, in 2012, Ramos et al. stated that the inhomogeneous distribution of built-up edges would lead to an increase of surface roughness [17]. Three years later, Huo et al. [18] used the Raman spectrum of silicon to measure the absolute values of the intensity from different scans varying due to the non-uniformity of a surface. In 2018, Sun et al. developed a method to quantitatively evaluate micro-milled surface non-uniformity [19]. In the same year, Sun et al. further pointed out that changes with the tool rotation inevitably cause the non-uniformity of the surface quality in micro-milling [5]. Although researchers have known that milling can cause surface non-uniformities, there has been little research mentioning that longitudinal-torsional coupled UVAM can improve Ti-6Al-4V alloy surface homogenization.

While researching longitudinal-torsional (L-T) coupled ultrasonic vibration milling, Amini et al. recently investigated the performance of L-T vibration during ultrasonic-assisted drilling of Al 7075 [20]. In a similar process, Paktinat et al. designed a longitudinal-torsional ultrasonic-assisted drilling (L-T UAD) AISI 1045, and they compared the effects of conventional drilling, longitudinal ultrasonic drilling, and L-T UAD [21]. In addition to applying the L-T coupled ultrasonic technique on metal material as a typical progression for non-metallic material, in 2015, Asami et al. developed a new method that used an abrasive slurry and ultrasonic composite vibration to produce L-T vibrations for the processing of soda-lime glass [20]. Three years later, Wang et al. proposed a new type of L-T coupled vibration to further improve the processing performance of rotary ultrasonic machining for quartz glass [22]. In another year, Xiang et al. further developed the L-T vibration-assisted cutting process for honeycomb core composite material [23]. In addition to drilling and grinding, L-T coupled vibrations also have important applications in milling. For the last 2 years, Wu et al. have conducted ultrasonic vibration milling experiments that show that the L-T ultrasonic vibration transducer plays a big role in the cutting process. Compared to CM, UVAM vibration milling greatly reduces cutting forces [24]. Niu et al. further superimposed the L-T ultrasonic vibration on the milling of Ti-6Al-4V alloy [25]. However, although L-T coupled ultrasonic vibration has many advantages, a decrease in the torsional stiffness can also have a negative effect on processing.

Suárez et al. illustrated the positive effect of UVAM with the important effects of the ultrasonic vibration-assisted milling of Ni-Alloy 718 [26]. For the same situation, the experimental results of the average cutting force were decreased using UVAM in the recent research of Zarchi et al. [27]. Later, a vibration of the cutting tool was reported that could lead to a high reduction of the cutting forces [28]. In addition, Tao et al. proposed a kinematic model for defining the formation mechanism of the surface texture in the feed-direction UVAM process [29]. Moreover, the surface residual stress and the hidden integrity effects of UVAM were also studied in [30, 31]. However, almost none of the research paid attention to the overlapping machining area with a ball-end cutting miller in the UVAM process.

As discussed above, UVAM has some advancements and limitations, and little research work has been done on the homogenization of surface of ball-end milling with UVAM. Hence, this study reports on the changing process of the ball-end milling surface roughness value determined by the UVAM and CM processes in an overlapping area. In this area, some of the cutting surface integrity values for the ball-end are compared for CM and UVAM. In Section 2, an experimental procedure is designed in which the materials, setup, characterizations, and cutting method are introduced and analyzed. Then, in Section 3, the cutting experiments are carried out, the cutting forces are further analyzed, and the roughness and topography of the finished surfaces are discussed. Finally, the conclusions regarding the UVAM method in the machining process are given.

2 Experimental procedure

2.1 Materials

The workpiece was made of a Ti-6Al-4V alloy. The workpiece had the dimensions of $80 \times 34 \times 10$ mm^3, and it was cut by wire electrical discharge machining. The operation area of the machine was set to 60×34 mm^2, which allowed the simultaneous performance of eight different slot experiments using a ball-end milling cutter with the same tool coating. There were generally two flues on the ball-end milling cutter: (i) The residuals on the workpiece surface and (ii) the oxide layer on the workpiece surface. Therefore, the workpiece was first cleaned by an ultrasonic cleaner immersed in alcohol and then it was dried in the air before measurement to remove the residuals adhered to the surface, thus avoiding chemical interaction with the oxygen in the air. The material properties of Ti-6Al-4V are listed in Table 1. To machine the overlapping

Table 1 Material properties of Ti-6Al-4V

Property	Unit	Value
Density	kg/m^3	4510
Hardness (Rockwell)	HRC	36
Elastic modulus	GPa	113.8
Tensile strength	MPa	950
Melting temperature	°C	1660

machining area surface point-by-point under the ultrasonic process, the value of Δ_p was set to 100 μm.

2.2 Experimental setup

Figure 1 illustrates a schematic system of the ball-end milling experiments. The system was composed of three main parts: a numerical control milling sub-system, an ultrasonic vibration sub-system, and a cutting force data acquisition sub-system.

A milling sub-system (Haas, VF-1, USA) was used to conduct all of the experiments in both the UVAM and CM processes, for which the numerical control (NC) milling machine system had a three-axis milling configuration. The *X*-axis, *Y*-axis, and *Z*-axis, as well as the rotation of the spindle axis of the *Z*-axis could be controlled by the NC program and the cutting experiments were conducted in a no-coolant condition. The ultrasonic vibration sub-system was composed of a transducer cutting force data acquisition sub-system was composed of a Kistler dynamometer and a VibRunner acquisition system. Because the UVAM system had a variable depth of cut, the cutting speed V_c was also a variable parameter; this calculation is detailed in the Supporting Information. For this milling system, the cutting parameters were set as shown in Table 2.

2.3 Characterizations

The surfaces were machined by the UVAM and CM processes and further characterized by many instruments. First, the surface roughness value was measured by a surface profilometer (Mahr, MarSurf LD 120, Germany). Then the cutting force was in situ measured with a newly established measurement system in which a calibrated Dynamometer (9256CQ01, Kistler Inc., Switzerland) was used to measure the cutting force and the digital signal was collected by VibRunner (m+p international, Germany) data acquisition card. The morphology features of the cutting chips were

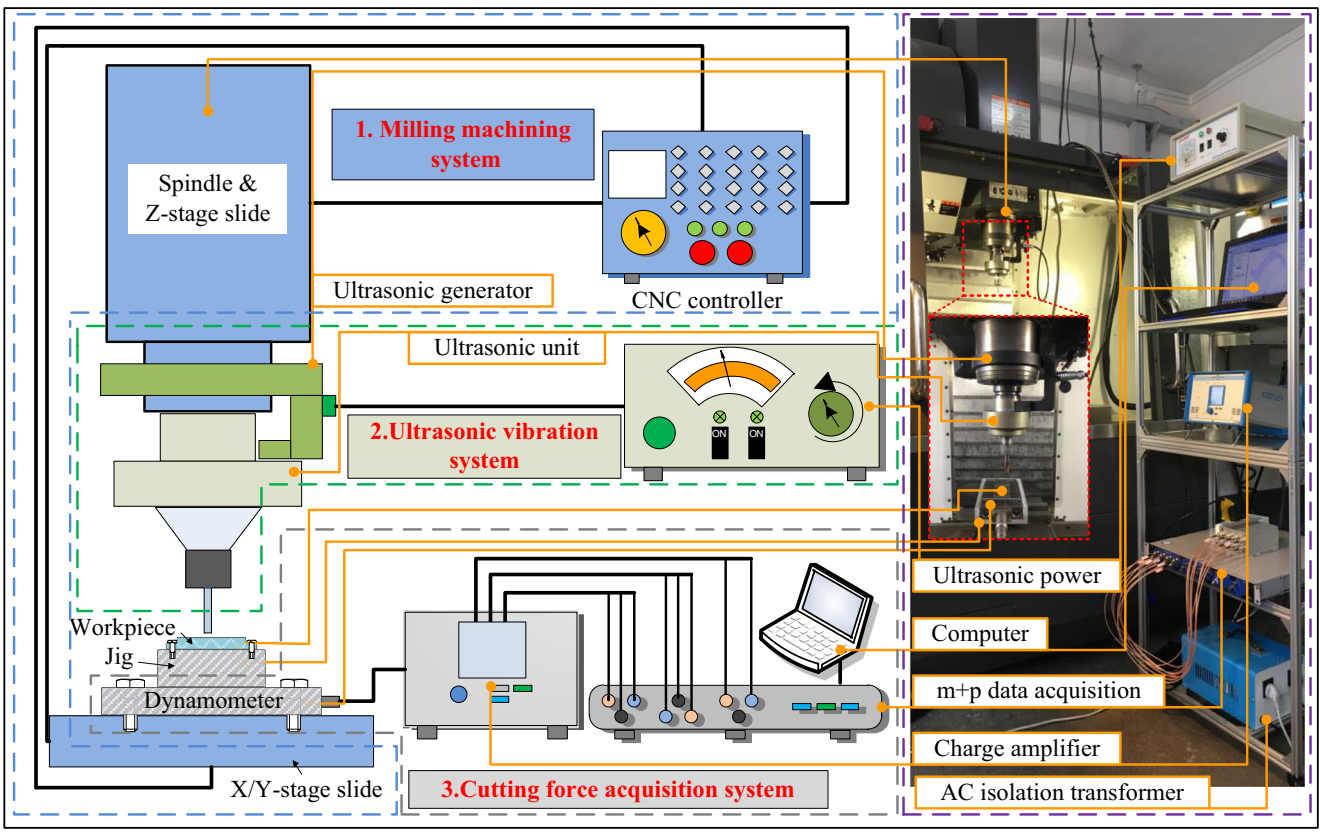

Fig. 1 The scheme of UVAM and CM experimental system: part 1 is the a numerical control milling sub-system; part 2 is the ultrasonic vibration sub-system; and part 3 is the cutting force data acquisition sub-system

Table 2 Major experimental conditions

Parameter	Unit	Value
Vibration frequency (f)	kHz	About 25
Vibration amplitude (A)	μm	5.6
Spindle speed (n)	rpm	3000, 4000, 5000, 6000
Max cutting speed (V_c)	m/min	94.2, 125.6, 157, 188.4
Feed rate ($V_f = f_z \times Z \times n$)	mm/min	100, 200, 300, 400
Depth of cut (a_p)	μm	20, 40, 60, 80
Diameter of tool (d)	mm	10
Feed per tooth (f_z)	mm/rev ▪th	0.017, 0.025, 0.03, 0.033
Path interval (Δ_p)	μm	100
Coolant	/	None

characterized using a scanning electron microscope (SEM) (ZEISS, EVO 20, Germany). The surface morphology was captured by a digital microscope with an ultradepth of field digital microscope (ZEISS, Smartzoom5, Germany). The residual height detail was captured by a laser scanning confocal microscope (ZEISS, LSM700, Germany).

2.4 Cutting methods

To analyze the cause of the surface homogenization, the cutting zone and the principle of the ball-end milling performed by the UVAM and CM processes are described in Figs. 2 and 3, respectively, where two directions are taken into consideration in the machining process.

In the longitudinal direction, along with the feed rate direction of the milling cutter, the surface roughness and topography mainly depended on the tool diameter and the feeding rate. h_L (defined in the Supporting Information) represents the cutting residual height of the surface. In the transverse direction, as shown in Fig. 3a, Δ_p and R represent the key factors influencing the roughness and topography of the transverse surface. The overlapping area of the tool paths was an important parameter. The diameter of the milling cutter was 10 mm and Δ_p was 100 μm. Thus, almost the entire surface was machined by overlapping milling. h_T represents the residual height of the surface along the longitudinal direction. In this paper, the homogenization of the machined surface in two directions contains the surface roughness and the topography measurements. According to the geometric relationship seen

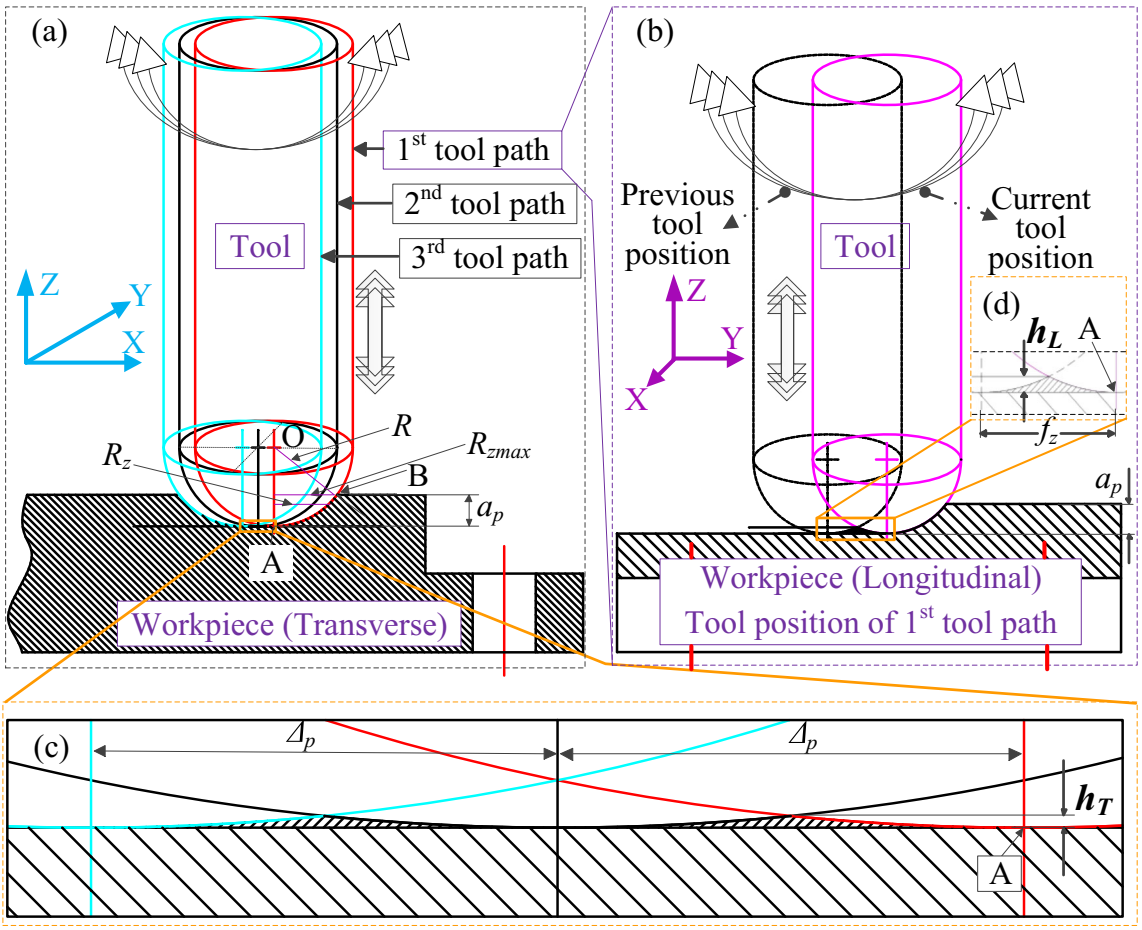

Fig. 2 The cutting principle of ball-end milling. **a** The transverse residual height display (in X direction). **b** The longitudinal residual height display (in Y direction). **c** The longitudinal residual height display in detail. **d** The transverse residual height display in detail

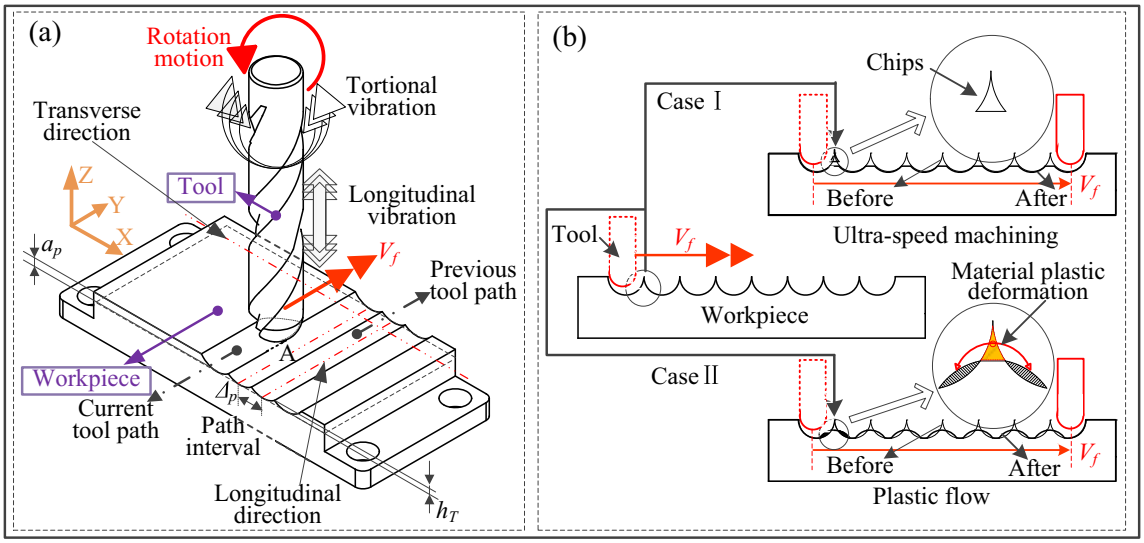

Fig. 3 Cutting principle. **a** Ball-end milling cutting principle of UVAM. **b** The two models of UVAM secondary processing: case I: ultra-speed machining; case II: material plastic deformation

in the Fig. 2, H integrates h_L and h_T together in the following formula. H is the residual height:

$$H = R - \frac{1}{2}\sqrt{4R^2 - \alpha^2}, \alpha = \begin{cases} f_z & (H = h_L) \\ \Delta_p & (H = h_T) \end{cases} \quad (1)$$

where f_z is the feed per tooth, Δ_p is the path interval, and R the radius of the ball-end. Therefore, the values of f_z and Δ_p are the important parameters in the calculation of the surface residual height.

It was found that the assisted feed-direction ultrasonic vibration could drive a separate-type milling that was different from conventional operation with the use of a reasonable parameter-matching condition. The maximum valid radius of the cutting tool was calculated, and the difference in the cutting process between the UVAM and CM processes is shown in the Supporting Information. In addition, in the ultrasonic vibration-assisted process, a high-frequency instantaneous acceleration would form on the endpoint of the ball-end miller, lowering the large vibration residual stress existing inside the material. There were two cases in the ball-end milling process related to the finished surface: roughness and topography.

Case I: The peak value of the residual height (the values of h_L and h_T) was calculated in the Supporting Information for the surface machined by both the CM and UVAM processes. In this case, the ultrasonic ultrahigh-speed milling process was the same as the grinding process, as illustrated by the top figure in Fig. 3b.

Case II: The peak of the residual height (the values of h_L and h_T) on the surface was treated as an entity that could be plastically deformed to some extent, so we had reasons to believe that the ultrasonic effect enhanced the stiffness of the cutter. Because the velocity in the center of the milling cutter was zero (the rotation radii were zero), the center point of the ball-end milling cutter did not participate in the cutting motion. This motion is also illustrated with the bottom figure in Fig. 3b. Moreover, the rigid cutter end would squeeze the surface in the same way as a high-frequency hammering action under UVAM, and the peak of the residual height would be squeezed into the valley between two peaks on the surface of the microarea.

3 Results and discussion

3.1 Finished surface roughness

In total, the surface roughness measurements of 256 groups were carried out along both the longitudinal and transverse directions with and without ultrasonic assistance. The surface machined by UVAM had an almost overlapping area according to the small value path interval Δ_p and the tens of microns cutting depth. Figure 4 shows the comparison of the surface roughness for the ball-end milling of Ti-6Al-4V with the UVAM and CM processes along the longitudinal and transverse directions. The solid curves in the figure denote the Ra of the UVAM process, the red curve with the circles represents the Ra of the transverse direction, and the green curve with squares represents the Ra of the longitudinal direction. It should be noted that in the UVAM process, the Ra value was 0.668 μm at 3000–4000 rpm. Conversely, the Ra value decreased to 0.161 μm at 5000–6000 rpm. As seen in Fig. 4, the Ra value of the UVAM process at 5000–6000 rpm was obviously lower than the CM value of the same parameter. However, this phenomenon did not reappear at the spindle speed range of 3000–4000 rpm. In the UVAM process, the machined surface was uniform and the transverse Ra was less than the longitudinal Ra under almost all of the parameters.

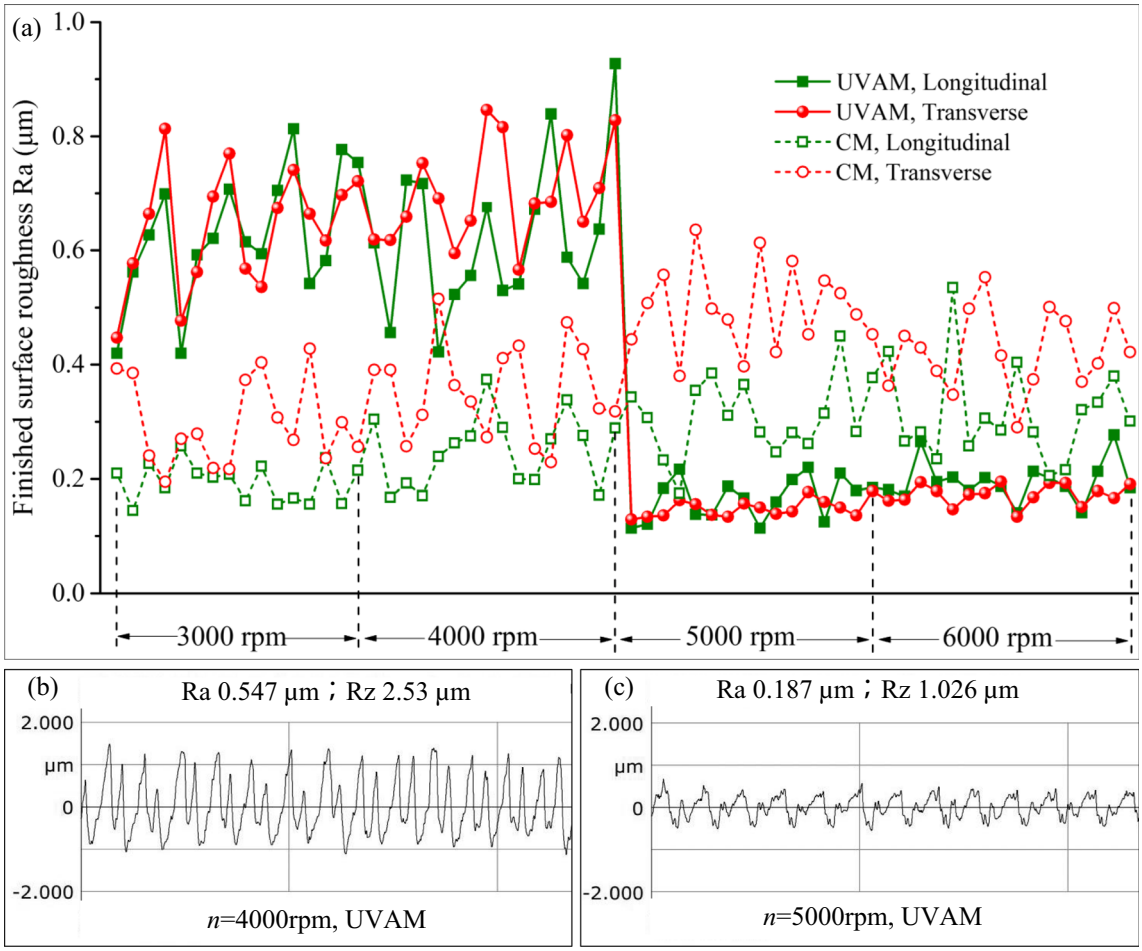

Fig. 4 Finished surface roughness comparison between UVAM and CM. **a** The whole surface roughness value of 256 groups contains longitudinal and transverse directions. The solid curves are roughness of UVAM process, and the dashed curves are roughness of CM process. The *X*-axis direction denotes the spindle speed with 4 intervals from 3000 to 6000 rpm. Every spindle speed contains 4 feeding rate, and every feed rate contains 4 depth of cut. This figure has further explanation in the Supporting Information. **b** The single parameter of surface roughness value in $n = 4000$ rpm, $V_f = 300$ mm/min, $a_p = 60$ μm. **c** The single parameter of surface roughness value in $n = 5000$ rpm, $V_f = 300$ mm/min, $a_p = 60$ μm

When spindle speed exceeded 5000 rpm, the Ra became smaller and more stable. It is worth noting that the surface roughness changed significantly in the UVAM process, from 4000 to 5000 rpm. Additionally, the roughness of the surface of the slots in the transverse direction had the same trend in the longitudinal direction.

Unlike the UVAM process, in the CM process, the surface had a relatively large deformation leading to inhomogeneous surface topography. The dashed curves denote the Ra in CM process, and the red circles represent the transverse direction, green squares representing longitudinal direction. Therefore, it can be concluded that the transverse Ra value was significantly higher than that of the longitudinal Ra value for almost all of the parameters.

According to an analysis of a large amount of the surface roughness data, UVAM process could increase the finished surface roughness for speeds under 4000 rpm (including 4000 rpm), while at speeds above 5000 rpm (including 5000 rpm), the UVAM process could decrease the finished surface roughness according to the spindle speed single tooth frequency of above 83.3 Hz, more matching the ultrasonic frequency (approximately 25 kHz). There were some causes for these surface roughness experimental results. With a higher spindle speed, the material removal mode with torsional vibration could change from shearing to squeezing. This result accords with the findings of the research of the reference [32], where the research results tended to reveal that the ultrasonic machining could enhance the surface roughness. However, the results of different researchers tended to reveal ultrasonic machining could reduce the surface roughness or at least not increase the surface roughness. With a spindle speed below 4000 rpm, Wang et al. [33] presented results that showed the ultrasonic vibration was not always producing a positive effect; sometimes, it was even producing a worse effect than the CM process at a certain frequency. When vibration was higher than 5000 rpm, the chips and cutting heat

could be easily reduced or completely eliminated, resulting in a more uniform surface with UVAM.

Figure 5 displays the surface roughness homogenization analysis of the UVAM and CM processes. It should be noted that when the ratio between the absolute value of the Ra minus the longitudinal Ra and longitudinal Ra was taken into account, the homogenization of the surface roughness significantly decreased in the UVAM process compared to the CM process. The difference of the homogenization of the UVAM, denoted with pink, was much lower than the CM difference, denoted in the green bar chart. It was found that the homogenization analysis of the roughness ratio in UVAM was 15.1%, while it was 59.4% in the CM process. Additionally, the average value curve fluctuation shown in the pink bar chart for the UVAM process was much smaller than the fluctuation for CM, shown in the green bar chart. After many surface roughness measurements, with the spindle speed increasing in UVAM, the surface quality had a significant improvement. The surface roughness experiments had limitations. It should be noted that this study conducted roughness measurements in only two orthogonal directions without considering the arbitrary directions.

According to this trend shown in the bar chart of Fig. 5, the UVAM process played a significant role in the uniformity of the surface. This was because UVAM was an intermittent milling process, and the time of the material shear deformation caused by the rotation of the tool occupied only a small section of entire cutting time. The larger the surface deformation was, the more uniform the surface was. Another reason for this was that the introduction of ultrasonic vibrations to the cutting region added a residual height h_L and reduced the residual height h_T value. The UVAM process decreased the height of both the h_L and h_T via 25,000 plastic deformations per second.

3.2 Cutting force measurement

The integrated cutting force at high frequency was measured in situ during the cutting process by a calibrated dynamometer. We combined the Kistler 6-component dynamometer 9256CQ01 and VibRunner acquisition card to obtain the data of the cutting force. This system was used to collect the cutting force data for both the UVAM and CM processes. The UVAM process worked at a frequency of approximate 25 kHz. To collect abundant data in a short time, the VibRunner data acquisition system was utilized. The cutting force mainly consisted of the three parts of the chip deformation force, friction force, and ultrasonic impact force for ball-end milling with an ultrasonic vibration-assisted process. Under the same cutting parameters, the cutting force of UVAM is smaller than the CM force, and the peak force mainly depended on the matching of three parameters: the spindle speed, feeding rate, and cutting depth. The data acquisition time of the cutting force was set to 20 s. Then the cutting force data were obtained from the steady cutting state in the process.

Figure 6 clearly illustrates the difference in the cutting forces for the UVAM and CM processes. Compared to the CM process, the average cutting force of the UVAM process was obviously lower in all three force directions. The directions of the three forces FX, FY, and FZ were consistent with the coordinates of X, Y, and Z in Fig. 3. As shown in Fig. 6a, d, g, the fluctuation range of the UVAM cutting force (the red curves) was obviously smaller than that of the range for the CM process (the black curves). The average value of FX in the UVAM process decreased by about 48.14% compared to the value for the CM process, as shown in Fig. 6a. Meanwhile, it is shown in Fig. 6d that the average value of *FY* was also reduced by about 21.04%. Further, it can be noted from Fig. 6g that the average value of FZ decreased by a large scale of about 35.76%. A cutting force fragment was selected for 12 s,

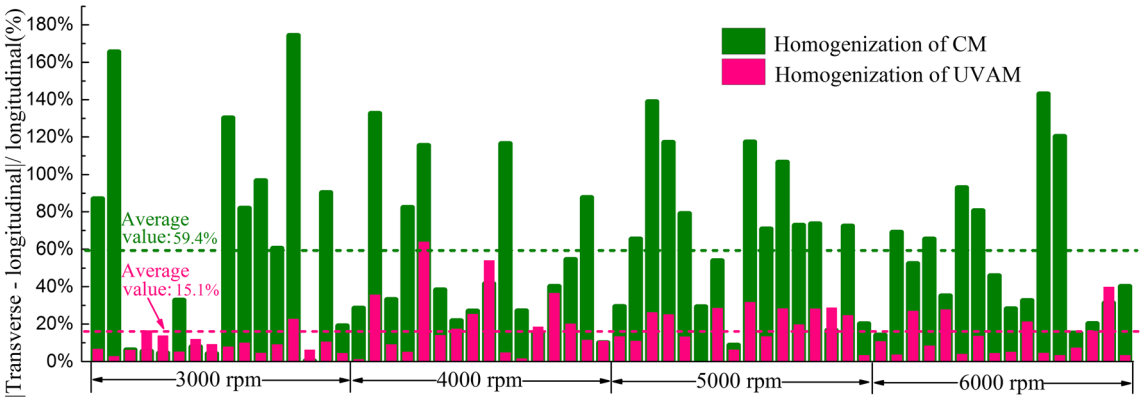

Fig. 5 Homogenization analysis of finished surface roughness: the *Y*-axis denotes homogenization value. The value is the ratio between absolute value of transverse Ra minus longitudinal Ra and longitudinal Ra. The *X*-axis denotes the 64 parameters including 4 spindle speed from 3000 to 6000 rpm, and every spindle speed contains 4 feeding rate from V_f = 100 mm/min to V_f = 400 mm/min with 4 intervals, and every feed rate cover 4 depth of cut 20 μm, 40 μm, 60 μm, and 80 μm. The average value of the homogenization in green bar is 59.4% in CM process; meanwhile, the average value of the homogenization in pink bar is 15.1% in UVAM process

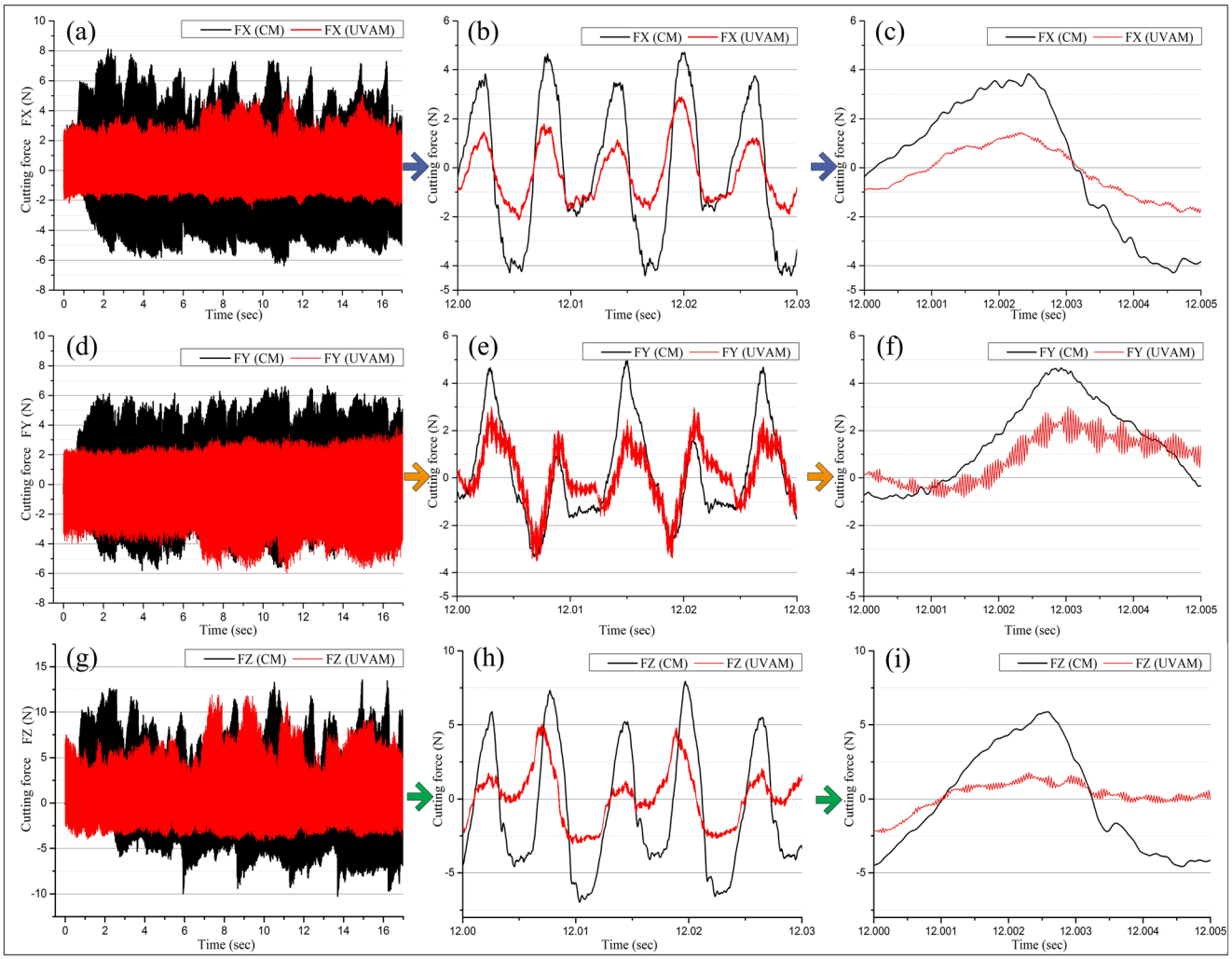

Fig. 6 The cutting force measurements of the UVAM and CM processes, where $n = 5000$ rpm, $V_f = 100$ mm/min, $a_p = 20$ μm. In these figures, the left, middle, and right columns are the displays of 17 s, 0.03 s, and 0.005 s, respectively, and the top, middle, and bottom rows stand for the cutting forces at *X*-axis (FX), *Y*-axis (FY), and *Z*-axis (FZ). **a** The cutting force along *X*-axis in 17 s. **b** The cutting force along X-axis in 0.03 s. **c** The cutting force along *X*-axis in 0.005 s. **d** The cutting force along *Y*-axis in 17 s. **e** The cutting force along *Y*-axis in 0.03 s. **f** The cutting force along *Y*-axis in 0.005 s. **g** The cutting force along *Z*-axis in 17 s. **h** The cutting force along *Z*-axis in 0.03 s. **i** The cutting force along *Z*-axis in 0.005 s

and the enlarged views of the data are displayed in Fig. 6b, e, h, where the cutting force peak-valley values are clearly compared between the two cutting methods. In the far-right column shown in Fig. 6, on the second level amplification view at the time of 12 s, it can be seen in detail that the ultrasonic vibration curve was different from the conventional curves, especially in those shown in Fig. 6f, i. The reason for this important observation was that the ultrasonic vibration component also had a positive effect on the cutting force reduction.

For this reason, the experimental result for cutting force decreased in UVAM. In the state of high-frequency separation in the UVAM process, the tool-workpiece net contact time was very short. A cutting force curve similar to a pulse was produced by the periodically intermittent separation of the tool and the microchip. Moreover, the UVAM process significantly released the cutting temperature of the cutting area via opening the dead zones and the effect of the thermal stress was reduced, further reducing the entire cutting force. Furthermore, another reason for the cutting force reduction was the fact that the torsional vibration would decrease the blade wedge angle of the tool in a short time [23].

Figure 7 shows the average cutting force at 5000 rpm with different feeding rates and cutting depths. The upper half of Fig. 7 shows the average cutting force with variable cutting depths. The lower part of Fig. 7 shows that the mean cutting force varied with the feed rate. It can be clearly seen that under the same parameters, almost all of the average cutting forces of UVAM were lower than the average cutting forces of CM. In Fig. 7a–d, the average cutting force is positively correlated to the cutting depth. The average cutting force value was a minimum at 20 μm and a maximum at 80 μm. There was an

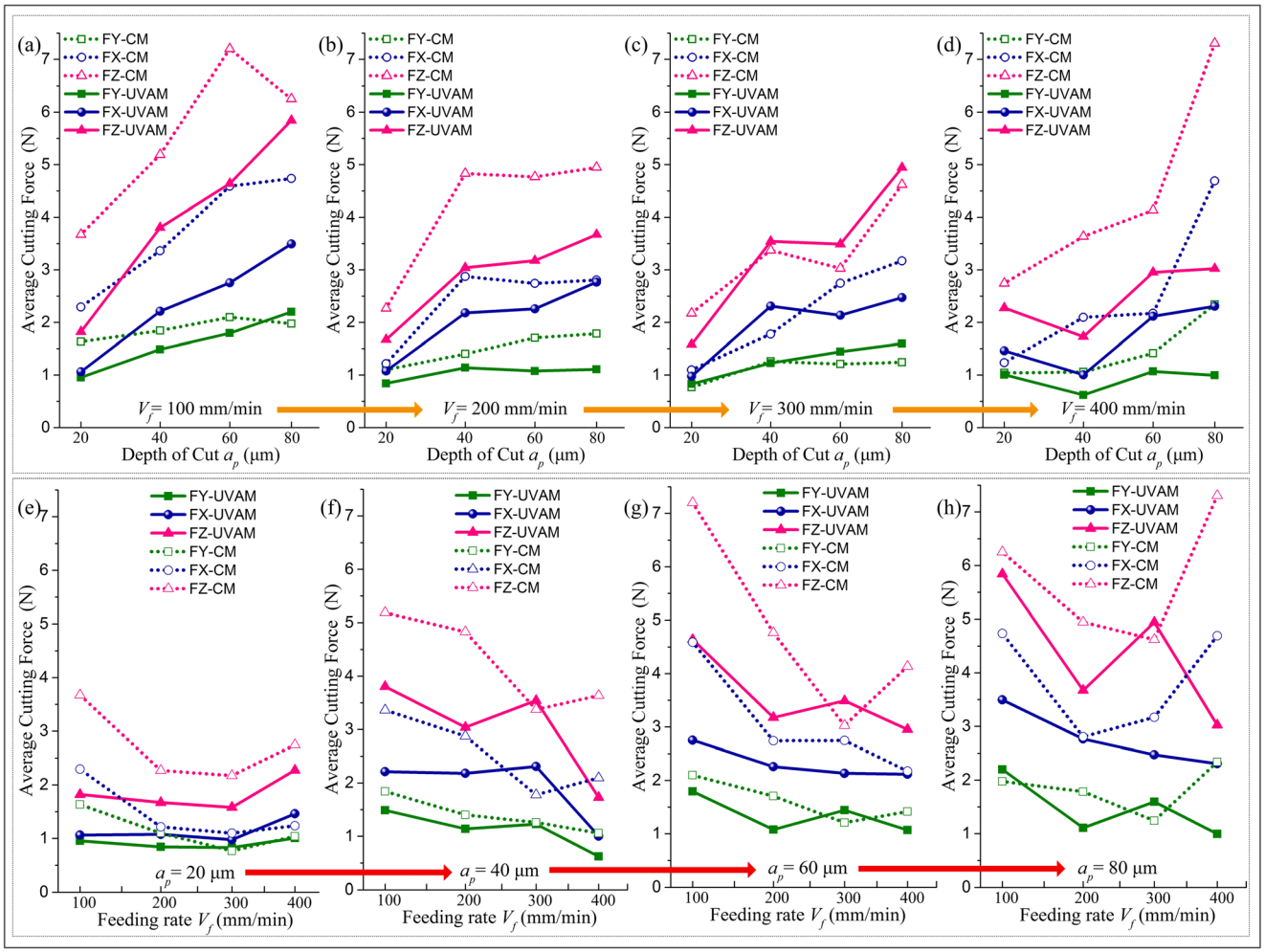

Fig. 7 The average value of cutting force both in UVAM and CM processes at 5000 rpm. **a**–**d** The certain feed rate (V_f) with varying cutting depth from 20 to 80 μm. **e**–**h** Certain cutting depth (a_p) with varying feed rate from 100 to 400 mm/min

abnormal situation for the feeding rate at 400 mm/min and the cutting depth at 40 μm. For the three directions, the *Y*-axis subjected to the smallest cutting force. For the *Z*-axis, along with the vibration direction, the material resistance cutting force was the largest in this direction. The maximum cutting force was 7.306 N, which appeared at V_f = 400 mm/min and a_p = 80 μm in the CM process, as shown in Fig. 7d. However, in the UVAM process, the maximum average force occurred at V_f = 100 mm/min and a_p = 80 μm. As displayed in the figure, the cutting depth was a main factor affecting the cutting force value. In ultrasonic assistance machining, frequency matching is very important, and there is a best-matching relationship between the ultrasonic frequency, spindle rotation frequency, and feeding rate frequency. In Fig. 7e–h, the average cutting force is negatively correlated to the feeding rate, which is especially clear in Fig. 7f, g. As shown in Fig. 7f, g, h, the cutting force of the CM process increased rapidly at 400 mm/min, and the cutting force in all three directions decreased significantly with the assistance of ultrasonic vibrations.

For the observation of average cutting force comparison between the UVAM and CM processes, the cutting miller oscillation was helpful for the material removal process. Moreover, there was a lower machining force in the UVAM process that created a shearing effect between the milling cutter and the finished surface when compared to the CM process. Furthermore, for the UVAM processing, the materials shear deformation caused by cutting was reduced, and the cutting force naturally decreased again.

Using an analysis of the homogenization of the cutting force in Table 3, the average value of the cutting force for the *X*- and *Y*-axes was calculated. The value was the ratio between absolute value of the transverse cutting force minus the longitudinal cutting force and the longitudinal cutting force. For the homogenization in UVAM, the transverse-longitudinal ratio was 40.45%. The transverse-longitudinal ratio in the CM process was 45.01%, which was larger than the value for the UVAM process. The above analysis demonstrates that the homogenization was not very significant for conducting the cutting force measurements.

Table 3 The homogenization of cutting force at 5000 rpm

Average value of cutting force at 5000 rpm	FX (N)	FY (N)	FZ (N)	FX − FY (N)	|FX − FY|/FX %
UVAM	2.225	1.325	3.458	0.9	40.45
CM	3.077	1.692	4.891	1.385	45.01

3.3 Chip analysis

As the most profound proof of the cutting force, Fig. 8 illustrates the SEM micrographs of some cutting chips that were fabricated with the cutting parameters of $n = 5000$ rpm, $V_f =$ 300 mm/min and the varying cutting depths a_p of 20–80 μm, for both the UVAM and CM processes. Figure 8a, e, i, m shows that the chips from the backside view in the CM process were more continuous than the chips in the UVAM process, which had a big deformation. It was difficult to break into the smaller chips, and it was difficult to distinguish the edges between chips. For the cutting chips, a fibrosis phenomenon was found in the inner circular surface where the transformation bands had obviously organizational refinement. An adiabatic shearing slip and plastic fracture dimples were found in the deformation zone. In particular, in the view of Fig. 8e, the cutting chip indicates not only the big deformation in the milling force but also the occurrence of some squeeze phenomenon in the surface materials at the same time as the larger cutting force. Consequently, this was another proof of the cutting deformation between the workpiece and the endpoint of the ball-end miller.

Figure 8a, e, i, m shows SEM graphs of cutting chips machined by the CM process in the red rectangle, and Fig. 8c, g, k, o shows the SEM graphs of chips machined by the UVAM process in the orange rectangle. As shown in Fig. 8, the chip size was more uniform for UVAM process than it was for the CM process, while the CM process generally induced a larger deformation and received a greater cutting force than the UVAM process. With the comparisons of the chip morphologies, the chip surface in the UVAM process appeared more uniform in accordance with the views of Fig. 8c, g, k, o.

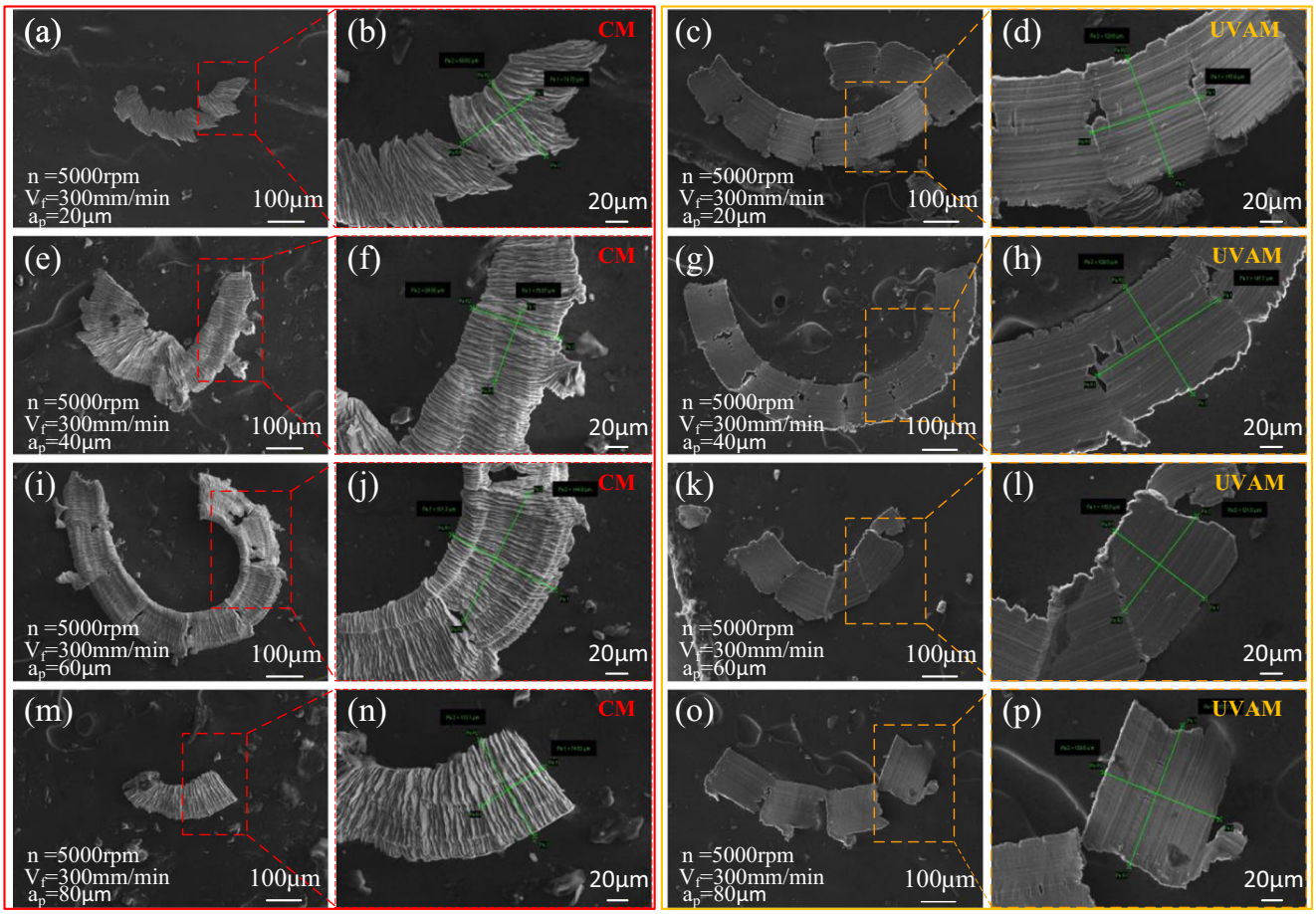

Fig. 8 The chips SEM micrographs both in UVAM and CM processes: **a**, **e**, **i**, **m** The CM process with varying cutting depth from 20 to 80 μm. **b**, **f**, **j**, **n** The enlarged view of CM process. **c**, **g**, **k**, **o** The UVAM process with varying cutting depth from 20 to 80 μm. **d**, **h**, **l**, **p** The enlarged view of UVAM process. Cutting constant parameters: $n = 5000$ rpm and $V_f =$ 300 mm/min

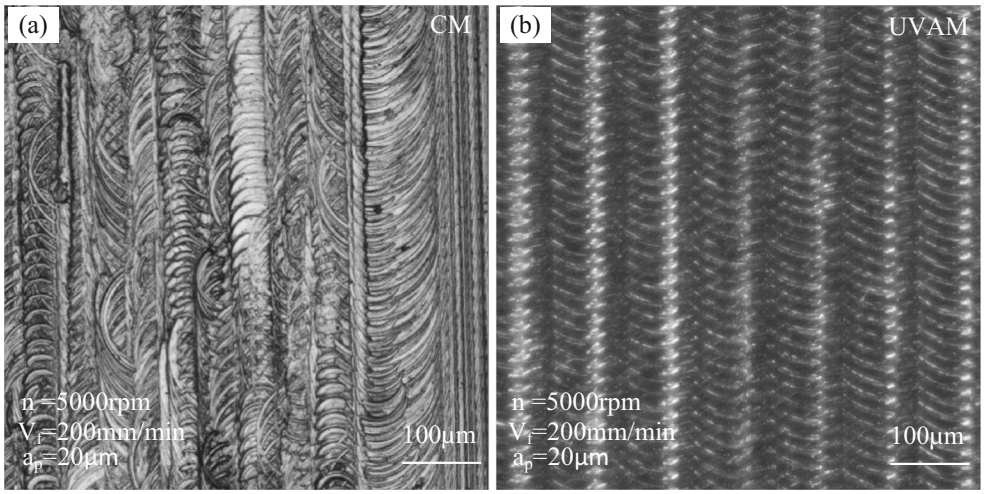

Fig. 9 The micrograph of slot-bottom surface by Smartzoom5 in detail. **a** The surface machined by CM process. **b** The surface machined by UVAM process. Cutting parameters: n = 5000 rpm, V_f = 200 mm/min, a_p = 20 μm

It can be seen from Fig. 8 that the chip in the left red rectangle was in a large deformation state. Additionally, the whole chip fragment was severely deformed, and the fragment edge was staggered, which was caused by the strongly cutting shear stresses. The chips in the orange rectangle on the right side were lightly deformed. The surface texture of the chips was more uniform, and the edge of the chips was smoother. The curvature of the whole chip fragment was small, and there were obviously fracture gaps between the adjacent chips that reflected the cutting process in a stable state. As the cutting depth a_p increased, the size of the chip did not change significantly in the CM process. However, in the UVAM process,

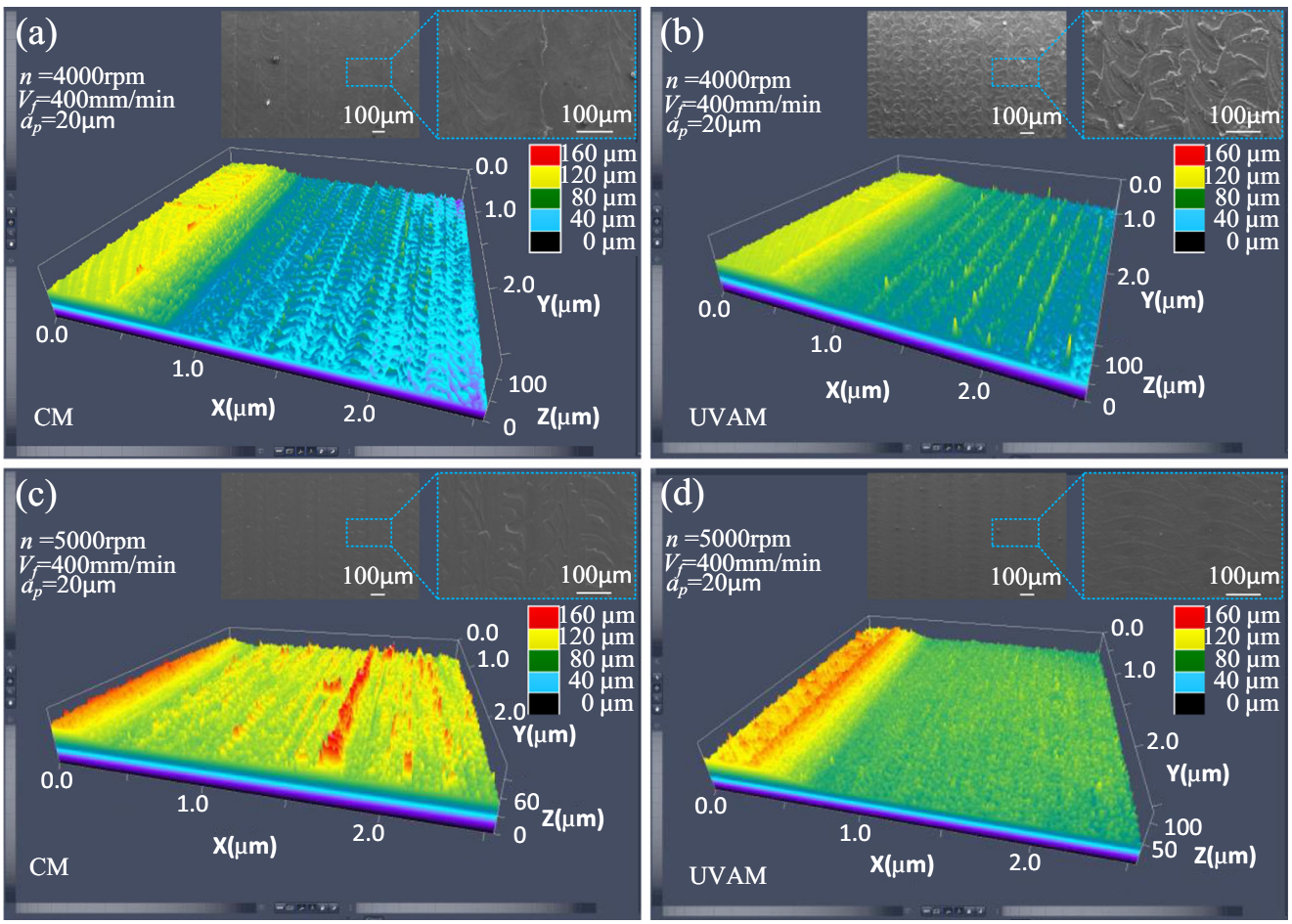

Fig. 10 The micrograph of topography of the bottom of slots by LSM700. **a** CM in n = 4000 rpm. **b** UVAM in n = 4000 rpm. **c** CM in n = 5000 rpm. **d** UVAM in n = 5000 rpm. Cutting constant parameters: V_f = 400 mm/min, a_p = 20 μm

with the increase of the cutting depth, the curvature of the entire chip became larger, and the gap between the chip units was enlarged, cracking further into an independent chip unit. However, the dimension of each chip did not obviously change.

The uniform chip morphology implied that the uniform machining surfaces and the strongly surface-deformed chip morphology also resulted in an uneven surface formation. This can be explained by the fact that the cutting tool oscillation added air to the gap between the tool and the chips. The whole chip fragment was severely deformed, and the fragment edge was staggered, which was caused by the strongly cutting shear stresses. Therefore, the temperature reduction was generated during the vibration of the tool in UVAM processing. Another cause was the torsional vibro-impact mechanism changes to the natural formation of the deformed chip, which caused the chip to tend to break [20]. Furthermore, the vibration amplitude affected the gap between the tool and the workpiece material, resulting in better chip-breaking conditions.

3.4 The surface topography analysis

As shown in Fig. 9, to observe the real appearance of the surface of the workpiece, the optical micrographs of the slot-bottom surface machined by the CM and UVAM processes were taken with Smartzoom5, and the parameters were set as $n = 5000$ rpm, $V_f = 200$ mm/min, $a_p = 20$ μm. There was a significant difference between these two manufacturing methods. In comparison, the micrograph of the slot-bottom surface with the vibration marks machined by the UVAM process was taken, as shown in Fig. 9.

In Fig. 9a, the surface cutting trace of the workpiece was very chaotic and messy when using the CM process, where a strong deformation occurred. This was another proof of plastic deformation in center point of ball-end mill in Section 2.4, implying a non-uniform friction, a high cutting force, and a rapid tool wear. While in Fig. 9b, the cutting mark is very regular and presenting a more uniform surface. It could be noted that the function of the ultrasonic assistance has increased the rigidity of the tool and reduced the cutting force. Furthermore, the UVAM process could reduce the surface inhomogeneous deformation on the surface of the workpiece.

To study 3D topographies of the slot-bottom surfaces machined by the above two methods, the micrographs were obtained by a confocal laser scanning microscope, LSM700, as shown in Fig. 10. There were four different machining methods at spindle speeds of 4000 rpm and 5000 rpm, with and without ultrasonic assistance. With a cutting depth of 20 μm, the trace of the cutting tool left on the surface was not uniform. The roughness at 4000 rpm without ultrasonic assistance is shown in Fig. 10a. However, with the same parameters as the CM method, the topography of the surface under the UVAM method also had a uniform defect that was similar to rows of seedlings on the surface deformed by the cutting interval residual height, as shown in Fig. 10b. In addition, the topography at 5000 rpm was not uniform and the roughness at 5000 rpm was lower than the roughness at 4000 rpm, as depicted in Fig. 10c. In comparison with Fig. 10a–c, the topography with ultrasonic vibration depicted in Fig. 10d was more homogeneous and the roughness was the lowest among the four images. Moreover, the surface homogenization effect in Fig. 10d was the most significant among all of the parameters.

4 Conclusions

This paper presents the homogenization and surface morphology of Ti-6Al-4V alloy machined by longitudinal-torsional coupled ultrasonic vibration ball-end milling, which produces regular surface textures. The conclusions of this study are as follows.

First, it is not necessary to tilt the spindle axis or exchange the tool at the whole precision milling junction of the flat surface and the freeform surface. Second, the UVAM process can increase the finished surface roughness under 5000 rpm, while above 5000 rpm, the UVAM process can decrease the finished surface roughness. Third, the cutting force was in situ measured during cutting by UVAM, and this force decreased by 20–40% compared to the CM process. Additionally, during the surface homogeneity study, it was found from the homogenization analysis that the roughness ratio in the UVAM process was 15.1%, while it was 59.4% in the CM process. Furthermore, the homogenization analysis determined that the cutting force ratio decreased from 45.01 to 40.45% with ultrasonic assistance.

Funding This work was supported by China-EU H2020 International Science and Technology Cooperation Programme (FabSurfWAR Nos. 2016YFE0112100 and 644971) and Jilin Province Science and Technology Development Program Supported Project (20180201057GX).

References

1. Milton C, Shaw (2005) Metal cutting principles. Oxford University Press 2, 9–14
2. Cong W, Pei Z (2015) Handbook of manufacturing engineering and technology, process of ultrasonic machining. Springer-Verlag London 45:1630–1648
3. Zhou M, Eow YT, Ngoi BKA, Lim EN (2003) Vibration-assisted precision machining of steel with PCD tools. Adv Manuf Proc 18(5):825–834
4. Nath C, Rahman M (2003) Effect of machining parameters in ultrasonic vibration cutting. Int J Mach Tools Manuf 48(9): 965–974
5. Sun Z, To, S (2018) Effect of machining parameters and tool wear on surface uniformity in micro-milling. Micromachines 9:268–282

6. Maurotto A, Wickramarachchi CT (2016) Experimental investigations on effects of frequency in ultrasonically-assisted end-milling of AISI 316L: a feasibility study. Ultrasonics 65:113–119
7. Maurotto A, Muhammad R, Roy A, Silberschmidt VV (2013) Enhanced ultrasonically assisted turning of a β-titanium alloy. Ultrasonics 53(7):1242–1250
8. Han JG, Lin JQ, Li ZG, Lu MM, Zhang JG (2018) Design and computational optimization of elliptical vibration-assisted cutting system with a novel flexure structure. IEEE T Ind Electron 66(2): 1151–1161
9. Babitsky VI, Kalashnikov AN, Meadows A, Wijesundara AAHP (2003) Ultrasonically assisted turning of aviation materials. J Mater Process Technol 132(1–3):157–167
10. Geng D, Zhang D, Xu Y, He F, Liu F (2014) Comparison of drill wear mechanism between rotary ultrasonic elliptical machining and conventional drilling of CFRP. J Reinf Plast Compos 33(9):797–809
11. Zhou M, Wang M, Dong G (2016) Experimental investigation on rotary ultrasonic face grinding of SiCp/Al composites. Adv Manuf Process 31(5):673–678
12. Zhu X, Lin B, Liu L, Luan Y (2016) Power transfer performance and cutting force effects of contactless energy transfer system for rotary ultrasonic grinding. IEEE T Ind Electron 63(5):2785–2795
13. Zhang X, Kornel FE, Yu T, Wang W (2016) Cutting forces in micro-end-milling processes. Int J Mach Tools Manuf 107:21–40
14. Fontaine M, Moufki A, Devillez A, Dudzinski D (2007) Modelling of cutting forces in ball-end milling with tool–surface inclination: part I: predictive force model and experimental validation. J Mater Process Technol 189(1):73–84
15. Buj-Corral I, Vivancos-Calvet J, Domínguez-Fernández A (2018) Surface topography in ball-end milling processes as a function of feed per tooth and radial depth of cut. Int J Mach Tools Manuf 53(1):151–159
16. Tangjitsitcharoen S, Thesniyom P, Ratanakuakangwan S (2014) Prediction of surface roughness in ball-end milling process by utilizing dynamic cutting force ratio. J Intell Manuf 28:1–9
17. Ramos AC, Autenrieth H, Strau T, Deuchert M, Hoffmeister J, Schulze V (2012) Characterization of the transition from ploughing to cutting in micro machining and evaluation of the minimum thickness of cut. J Mater Process Technol 212(3):594–600
18. Huo, D. H.; Lin, C.; Choong, Z. J.; Ketan;, Pancholi, K.; Degenaar, P. (2015). Surface and subsurface characterisation in micro-milling of monocrystalline silicon. The Int J Adv Manuf Tech, 81(5–8), 1319–1331
19. Sun ZW, To S, Zhang SJ, Zhang GQ (2018) Theoretical and experimental investigation into non-uniformity of surface generation in micro-milling. Int J Mech Sci
20. Amini S, Soleimani M, Paktinat H, Lotfi M (2017) Effect of longitudinal–torsional vibration in ultrasonic-assisted drilling. Mater Manuf Process 32(6):616–622
21. Paktinat H, Amini S (2018) Numerical and experimental studies of longitudinal and longitudinal-torsional vibrations in drilling of AISI 1045. The Int J Adv Manuf Tech 94(5–8):2577–2592
22. Wang J, Zhang J, Feng P, Guo P, Zhang Q (2018) Feasibility study of longitudinal–torsional-coupled rotary ultrasonic machining of brittle material. J Manuf Sci E-T ASME 140(5):051008
23. Xiang D, Wu B, Yao Y, Liu Z, Feng H (2019) Ultrasonic longitudinal-torsional vibration-assisted cutting of Nomex® honeycomb-core composites. The Int J Adv Manuf Tech 100(5–8):1521–1530
24. Wu C, Chen S, Cheng K, Ding H, Xiao C (2018) Innovative design and analysis of a longitudinal-torsional transducer with the shared node plane applied for ultrasonic assisted milling. P I Mech Eng C-J Mec:0954406218797962
25. Niu Y, Jiao F, Zhao B, Wang D (2017) Multiobjective optimization of processing parameters in longitudinal-torsion ultrasonic assisted milling of Ti-6Al-4V. The Int J Adv Manuf Tech 93(9–12):4345–4356
26. Suárez A, Veiga F, Lacalle LNLD, Polvorosa R, Lutze S, Wretland A (2016) Effects of ultrasonics-assisted face milling on surface integrity and fatigue life of Ni-alloy 718. J Mater Eng Perform 25(11):5076–5086
27. Zarchi MMA, Razfar MR, Abdullah A (2013) Influence of ultrasonic vibrations on side milling of AISI 420 stainless steel. Int J Adv Manuf Technol 66(1–4):83–89
28. Ma CX, Shamoto E, Moriwaki T (2004) Study on the thrust cutting force in ultrasonic elliptical vibration cutting. Mater Sci Forum 471-472:396–400
29. Tao G, Ma C, Bai L, Shen X, Zhang J (2016) Feed-direction ultrasonic vibration assisted milling surface texture formation. Adv Manuf Proce 32(2):193–198
30. Yao Z, Kima GY, Faidley LA, Zou Q, Mei D, Chen Z (2012) Acoustic softening and residual hardening in aluminum: modeling and experiments. Int J Plast 39(39):75–87
31. Hampa PS, Razfar MR, Malaki M, Maleki A (2015) The role of dry aero-acoustical lubrication and material softening in ultrasonically assisted milling of difficult-to-cut AISI 304 steels. T Indian I Metals 68(1):43–49
32. Feng P, Wang J, Zhang J, Zhijun WU (2017) Research status and future prospects of rotary ultrasonic machining of hard and brittle materials. Chin J Mech Eng-En 53(19):3–21
33. Wang Y, Gong H, Fang FZ, Ni H (2016) Kinematic view of the cutting mechanism of rotary ultrasonic machining by using spiral cutting tools [J]. The Int J Adv Manuf Tech 83(1–4):461–474